

Absence of conventional room-temperature superconductivity at high pressure in carbon-doped H₃S

Tianchun Wang ^{1,*}, Motoaki Hirayama,^{1,2} Takuya Nomoto ¹, Takashi Koretsune ³,
Ryotaro Arita ^{1,2} and José A. Flores-Livas ^{4,2,†}

¹*Department of Applied Physics, University of Tokyo, Tokyo 113-8656, Japan*

²*RIKEN Center for Emergent Matter Science, 2-1 Hirosawa, Wako 351-0198, Japan*

³*Department of Physics, Tohoku University, 6-3 Aza-Aoba, Sendai 980-8578 Japan*

⁴*Dipartimento di Fisica, Università di Roma La Sapienza, Piazzale Aldo Moro 5, I-00185 Roma, Italy*



(Received 12 April 2021; revised 12 August 2021; accepted 12 August 2021; published 25 August 2021)

In this paper, we show that the same theoretical tools that successfully explain other hydride systems under pressure seem to be at odds with the recently claimed conventional room-temperature superconductivity of carbonaceous sulfur hydride. We support our conclusions with (i) the absence of a dominant low-enthalpy stoichiometry and crystal structure in the ternary phase diagram. (ii) Only the thermodynamics of C-doping phases appears to be marginally competing in enthalpy against H₃S. (iii) Accurate results of the transition temperature given by *ab initio* Migdal-Eliashberg calculations differ by more than 110 K from recent theoretical claims explaining the high-temperature superconductivity in carbonaceous hydrogen sulfide. An unconventional mechanism of superconductivity or a breakdown of current theories in this system is possibly behind the disagreement.

DOI: [10.1103/PhysRevB.104.064510](https://doi.org/10.1103/PhysRevB.104.064510)

I. INTRODUCTION

Over the last decade, pressurized hydride compounds have led the path to many important landmarks in superconductivity. Notable cases include silane in 2008 [1], H₃S in 2014 [2,3], which has triggered most of the field, and the confirmation of high T_c in LaH₁₀ by independent teams in 2019 [4–6]. This unfolding success of important breakthroughs is largely due to the symbiosis of theory, computation, and experimental sciences, which has accelerated the discovery by pointing to niches of interesting systems [7–11].

Recently, Snider *et al.* [12] achieved a decades-old quest; they reported solid evidence of the first room-temperature superconductor (RTS) made of carbon, sulfur, and hydrogen. Although the report set a landmark in the annals of science, there are still many open questions surrounding this important discovery. For instance, the exact stoichiometry of the claimed carbonaceous hydrogen sulfide that exhibits RTS is still elusive. Moreover, there is a debate with confronted arguments on the possibility of unusual superconducting features in all superhydrides at odds with the Bardeen-Cooper-Schrieffer theory [13–15]. It includes the sharp drop of electric resistivity at T_c and its dependence on a magnetic field [13,16,17]. It is worth noticing that the room-temperature superconductor reported at 287.7 K at 267 GPa has not been confirmed by magnetic susceptibility measurements [12]. But, amidst such unsolved puzzles, perhaps the most intriguing question regards the crystalline structure of the RTS.

Certainly, it is difficult to measure the crystalline structure of a tiny sample under extremely high pressure, addition-

ally complicated by the small scattering ratio of low- Z hydrogen. Hence, to clarify the mechanism of superconductivity and electronic and phonon properties, it is highly desirable to know the crystalline structure from the theoretical side. So far, there have been two works on crystal structure prediction for C-S-H ternary systems [18,19]. In these works, plausible structures were explored under high pressures $p = 100$ GPa [18] and 100–200 GPa [19], which reported many structure candidates for high- T_c superconductivity, including CSH₇. However, these candidates are *not* thermodynamically stable, and also the pressure explored is much lower than $p \sim 270$ GPa, at which the RTS was reported.

In this paper, we shed light on different open issues of the RTS. Resorting to structure prediction, we enlarged the chemical composition search and estimated the C-S-H ternary systems' formation enthalpy at 250 GPa. We also analyzed the doped phases, from their thermodynamic stability to superconducting properties and found flagrant differences compared to recent theoretical reports on C-doped H₃S [20,21]. On the transition temperatures obtained within virtual crystal approximation (VCA) and McMillan-Allen-Dynes (MAD) theory, presumably, an electronic smearing parameter holds to overestimate T_c 's theoretical value. In contrast, we found a more than 110 K difference in T_c between the experimental and the converged *ab initio* values. Our theoretical results show that the room-temperature superconductor cannot be explained by conventional superconductivity of carbon-doped H₃S phases nor other stoichiometries explored so far.

II. THERMODYNAMIC STABILITY

Due to the prohibited computational overhead of calculating a huge number of available compositions in the ternary system, we focus our strategy on exploring only representative

*tcwang@g.ecc.u-tokyo.ac.jp

†jose.flores@uniroma1.it

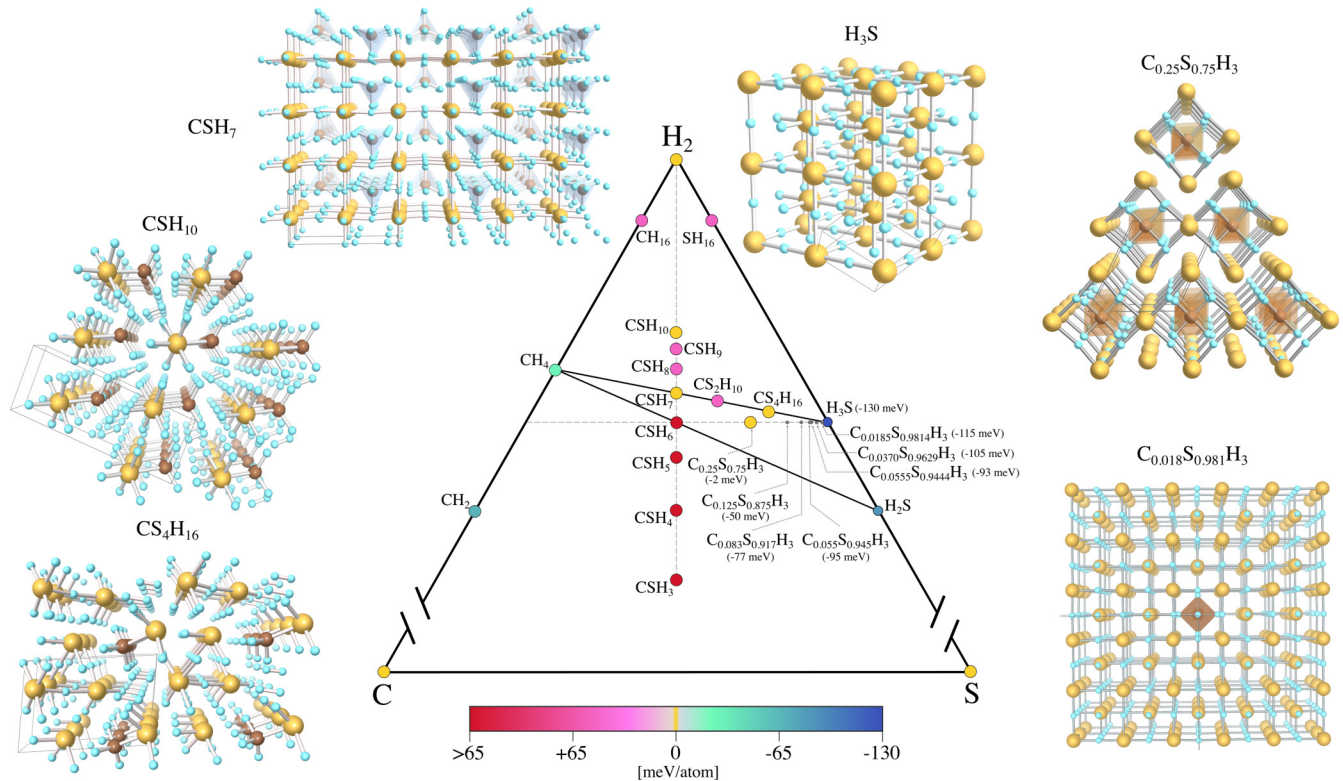


FIG. 1. C-S-H convex hull of the formation enthalpy calculated for selected stoichiometries at 250 GPa. Elemental phases and other low-lying enthalpy compositions are colored in yellow, in red, unstable, and from blue to dark blue, chemical compositions with negative formation enthalpy. At this pressure, the lowest enthalpy phase is H_3S (130 meV), followed by doped phases. However, already at 3.7% of C incorporation, the enthalpy difference between the parental phase and the doped one changes by 25 meV or ~ 290 K. Representative low-enthalpy structures of selected compositions are displayed outside the ternary hull. Intriguingly, in all the different regions studied in the phase diagram, the motifs with the lowest enthalpy correspond to molecular parts, either H_xC and H_xS , but nothing points towards a *fused*, covalently bonded C-S-H compound.

sections of the compositional landscape in detail. Figure 1 shows the C-S-H ternary convex hull for selected compositions at 250 GPa (see details in Ref. [22]; structures of compositions included in the phase diagram are listed in Ref. [23]; detailed information on the convex hull is provided in the Supplemental Material [24]). The zero-point energy (ZPE) is not included in the formation enthalpy calculation, since the ZPE contribution is usually at an energy scale of ~ 5 meV at a high pressure of 250 GPa, and it is hardly comparable to the scale of formation enthalpy ~ 100 meV [25]. We find CSH_7 (enthalpy of formation ~ 0 meV) and the absence of a dominant (low-enthalpy) phase, which is in agreement with previous works [18,19]. In our searches, we observed that different sections of the compositional space were governed by anticipated trends.

The high content of carbon and hydrogen (top left areas of the formation enthalpy triangle) will form CH_2 and CH_4 . Increasing hydrogen content (H_{5-16}) in these areas will then produce a phase separation to H_2 and CH_x , which are compositions with a formation enthalpy well above 100 meV/atom (not shown). In the middle section of the triangle, for C and S in a 1:1 ratio with increasing H (H_3 , H_4 , H_5 , and H_6), these stoichiometries are highly energetic and unlikely to occur. In these phases, decompositions to H_2 , H_3S , or CH_x are seen.

CSH_7 and CSH_{10} are interesting compositions that become metastable due to their conformation and “poor” metallicity.

These compositions are formed by H_3S and CH_x units with a weak ionic bond [18,19] between them (detrimental to high- T_c phonon superconductivity). Increasing the hydrogen above H_{10} in the ternary compounds, C-H binaries, or S-H binaries also results in phase separation. Most of the found phases present simple patterns, and these can be classified almost as amorphous phases. At the ratio of $\text{C}_{0.25}\text{S}_{0.75}$, the same pattern emerges, shown in the plotted figure [$\text{C}_{0.25}\text{S}_{0.75}\text{H}_3$; the characteristic cubic arrangement of sulfur hydrogen with distinctive layers and enclosed CH_4 units (a poor metal)]. Moving to $\text{C}_{0.5}\text{S}$ and lower hydrogen (below H_2) content seems odd for high- T_c superconductivity since decreasing the hydrogen content reduces the chances of finding key ingredients: metallic phases with a light atomic mass. Explorations below the CSH_3 range with C point towards the C-C formation of stable covalent bonds; however, these are semiconducting phases. In sulfur-rich areas, S-S metallic phases are found. However, these are unlikely to be responsible for the RTS.

The region close to the lowest-enthalpy (H_3S) phase is the most relevant in the compositional space. The varying C doping into the matrix of H_3S (C substitution in S sites) is the most reasonable solution from the thermodynamical point of view: We report that enthalpy decreases from -2 meV/atom at 25% C to -50 for 12.5% C, to -77 meV/atom for 8.3% C, to -95 meV/atom for 5.5% C, and finally to -105 meV/atom for 3.7% C, and so on until reaching

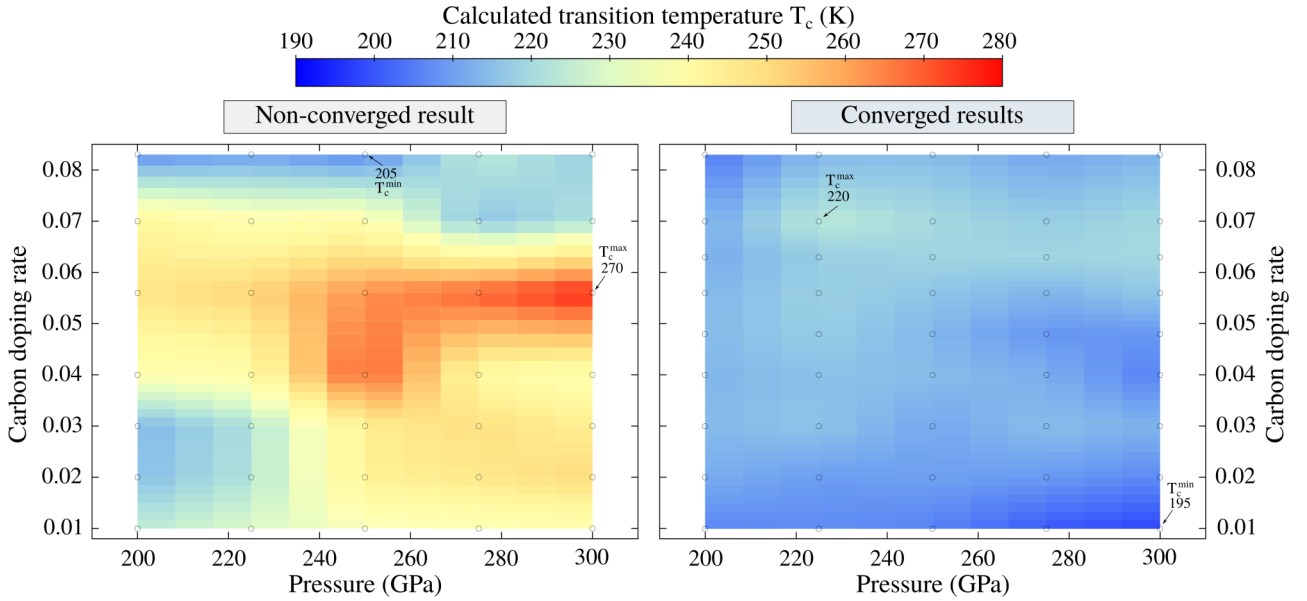


FIG. 2. Calculated doping-superconductivity-pressure phase diagrams using two protocols: The left panel shows T_c with a nonconverged parameter (see text) and the right panel with the controlled and converged protocol. The abscissa in both panels displays pressure in the range where the RTS was reported. The ordinate represents the carbon doping as simulated by the VCA and the color bar shows the estimated T_c given by the MAD formula. The Coulomb parameter μ^* is set to 0.1. Maximum and minimum T_c 's for each panel are shown. Beyond the technical validity of the VCA, it is clear that independently of doping and pressure, an RTS is absent for the converged case.

the H_3S with an enthalpy of -130 meV/atom (clearly the dominant composition). Judging by the convex hull of stability, C doping offers a possible structure model to explain the RTS, which is not new for other systems (see Ref. [7] for a review). Nevertheless, introducing carbon into the H_3S lattice comes at a price: It plays a detrimental role in single-phase stability (at 3.7% of the C-doping level, the enthalpy difference between the parental phase and the doped one changes by 25 meV or ~ 290 K), and excessive doping could also worsen the pristine electronic structure of H_3S .

III. SUPERCONDUCTING TRANSITION TEMPERATURE

It has been reported that, at least in the other two major systems (H_3S and LaH_{10}), the highly symmetric arrangements of atoms in hydrides under pressure display a van Hove singularity (VHS) near the Fermi level (E_F) [7,26]. In the case of H_3S (close to the C-S-H case), the VHS peak resides slightly lower than E_F [27]. From the electronic point of view, it is favorable for superconductivity to attempt electron doping. Recent studies based on the McMillan-Allen-Dynes (MAD) [28,29] formula have shown exceptionally that T_c of $\text{C}_x\text{S}_{1-x}\text{H}_3$ can be as high as room temperature when x is ~ 0.05 [20,21]. However, it is also well documented that the MAD formula is not a good approximation when the electron-phonon coupling is strong [30] or when the density of states (DOS) has a significant energy dependence around the VHS (as for electron doping) [30].

Let us first examine the effects of carrier doping onto the possible explanation of the RTS. Figure 2 confronts two phase diagrams of doping-pressure- T_c : The left one shows a pattern in the phase diagram with the maximum value of T_c reaching 270 K; the right panel (this work) shows quite the opposite phase diagram, with much lower T_c values. Though T_c as

high as 270 K occurs in the left plot, we note that this is a nonconverged result. Noticeably, when calculating the Eliashberg function $\alpha^2F(\omega)$, a sensitive parameter is the broadening width δ of the smearing for the double-delta integral. The left diagram in Fig. 2 is the result using the broadening width $\delta = 0.002$ Ry, and the right one is the result produced by $\delta = 0.014$ Ry. Since the results have significant dependence on the broadening width δ , to reach convergence, we choose the value of δ so that it can reproduce $N(0)$, where $N(0)$ is the DOS at the Fermi level given by the tetrahedron method [31] using a sufficiently dense mesh [32]. We ascribe the difference between the two plots in Fig. 2 from a lack of convergence; T_c is overestimated, especially with the MAD formula when too narrow smearing is used for the integral of the electron-phonon linewidth in the momentum space. The right panel summarizes T_c using a protocol and carefully tested electronic parameters [33] that reproduce theoretical values for H_3S [34] and LaH_{10} [6].

Besides the discussions above, another shortcoming of the MAD formula is the Coulomb interaction, which is introduced phenomenologically by a pseudo Coulomb parameter μ^* with a value set around 0.1. However, there is no reason why these values should be transferred at high pressure. In our case, the Migdal-Eliashberg (ME) calculation used the Coulomb interaction kernel, in which we solved the gap equation directly to get rid of μ^* . Thus, the ME calculation is more robust and straightforward, without any empirical parameters involved [33]. Using accurate first-principles Migdal-Eliashberg calculations [33,34] (see details in Ref. [35]), for which the doping effects are described by the VCA, we found that T_c 's of the doped phases of H_3S are hardly enhanced by ~ 20 K and decrease as a function of pressure (red line shown in Fig. 3). This tendency is also observed in H_3S [36–39] and LaH_{10} [6].

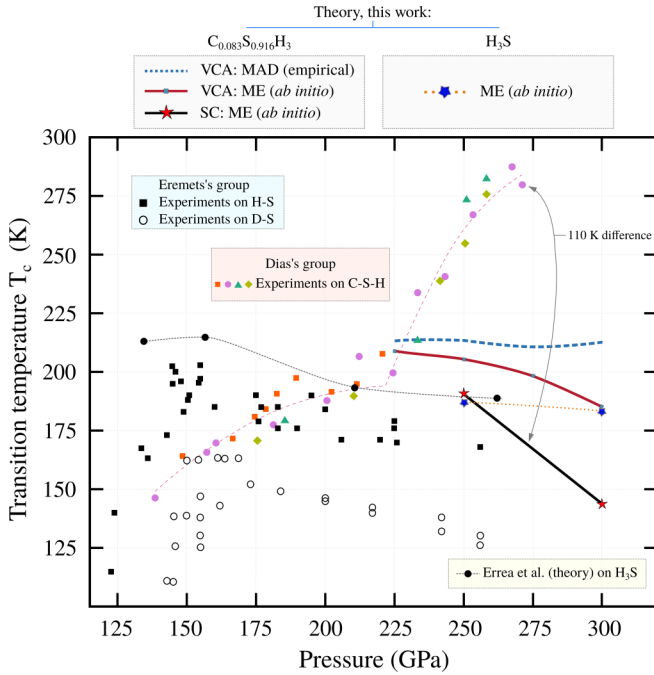


FIG. 3. T_c vs pressure: Theoretical results (this work) are estimated using different methods. Experimental results reported by Dias’s group on C-S-H [12], Eremets’s group on H-S and D-S [2,40,41], and theoretic results on H_3S [39] are also shown. Independent of the methodology used, our results suggest a sizable deviation as large as 110 K between the most reliable theoretical estimations and experiments on T_c (see details in Ref. [35] and Supplemental Material [24]).

In addition to the shortcomings of the MAD formula used in Fig. 2, another concern is the validity of VCA when mixing atomic potentials for non-neighboring species. The theoretical accuracy of VCA to estimate doping phase diagrams of hydrides under pressure is beyond the scope of this work. However, we would like to briefly discuss and compare the VCA and the supercell calculation, a more conventional scheme to treat the doping simulations. The VCA calculation is performed in the primitive unit cell (four atoms) and depends enormously on the atomic potential, alchemically constructed via a single virtual atom. For systems with a low doping ratio, the supercell contains 50–100 atoms. Compared to VCA, the supercell calculation is computationally costly, especially for the electron-phonon estimation. Nevertheless, it is presently the most accurate method for treating doping since it can capture electronic features and crystal symmetry breaking.

Figure 3 summarizes the up-to-date available values of T_c from experiments (Snider *et al.* [12]) and theory (this work).

We compare the supercell calculation with the one using the VCA approximation for estimations with C atom substitution. In Fig. 3, lines indicate the T_c dependence upon pressure calculated in this work with different levels of theory, from VCA (MAD formula), VCA (ME), and supercell (ME). It is noticeable that the level of theory employed does not play a role in describing what one could consider as an RTS. While the results given by the three methods are qualitatively consistent, they confirm the absence of RTS in carbon-doped phases of H_3S . In the same figure, we include the ME- T_c for H_3S and $C_xS_{1-x}H_3$ with $x = 8.3\%$. At 250 GPa, T_c is marginally increased by only ~ 5 K, and at 300 GPa, T_c for the C-doped phase is even lower than that of H_3S . The enhancement of superconductivity by C atoms, which has a lighter mass, is not significant because $C_xS_{1-x}H_3$ with a low doping ratio has a similar electronic structure and electron-phonon coupling characteristics as compared to H_3S . We refer the readers to the Supplemental Material [24] for extensive details on the electronic band structures, phonon density of states, and a thorough investigation of different doping models and how the electronic singularity is altered by carbon.

IV. CONCLUSIONS

Finally, we reach two contradicting points: On the one hand, doping appears to be the most likely explanation for the RTS. However, a low degree of doping does not alter the electronic structure, and T_c is close to the reported T_c of H_3S , as shown in Fig. 2. And on the other hand, large doping alters the so-called *fine-tuning* [12] of the VHS drastically.

In summary, from the thermodynamic perspective, substituting carbon in sulfur sites or interstitial space increases the formation enthalpy (it becomes less stable). Introducing carbon in the $Im\bar{3}m$ phase of H_3S plays against high T_c , changes the shape of DOS, decouples phonons, slightly modifies the lattice, and factors down T_c . Perhaps the current level of theory is insufficient to reconcile the scenario with the present experimental results. We conclude by asserting that in previous systems (H_3S [39] and LaH_{10} [6]), a remarkable compatibility between the theoretical and experimental sides in T_c and phase diagram is found; for the carbonaceous sulfur hydride, this might not be the case.

ACKNOWLEDGMENTS

We would like to thank M. Eremets for fruitful discussions. This work was supported by a Grant-in-Aid for Scientific Research (No. 19K14654 and No. 19H05825), “Program for Promoting Researches on the Supercomputer Fugaku” from MEXT, Japan.

- [1] M. Eremets, I. Trojan, S. Medvedev, J. Tse, and Y. Yao, *Science* **319**, 1506 (2008).
- [2] A. P. Drozdov, M. I. Eremets, I. A. Troyan, V. Ksenofontov, and S. I. Shylin, *Nature (London)* **525**, 73 (2015).
- [3] M. Einaga, M. Sakata, T. Ishikawa, K. Shimizu, M. I. Eremets, A. P. Drozdov, I. A. Troyan, N. Hirao, and Y. Ohishi, *Nat. Phys.* **12**, 835 (2016).

- [4] M. Somayazulu, M. Ahart, A. K. Mishra, Z. M. Geballe, M. Baldini, Y. Meng, V. V. Struzhkin, and R. J. Hemley, *Phys. Rev. Lett.* **122**, 027001 (2019).
- [5] A. P. Drozdov, P. P. Kong, V. S. Minkov, S. P. Besedin, M. A. Kuzovnikov, S. Mozaffari, L. Balicas, F. F. Balakirev, D. E. Graf, V. B. Prakapenka, E. Greenberg, D. A. Knyazev, M. Tkacz, and M. I. Eremets, *Nature (London)* **569**, 528 (2019).

- [6] I. Errea, F. Belli, L. Monacelli, A. Sanna, T. Koretsune, T. Tadano, R. Bianco, M. Calandra, R. Arita, F. Mauri, and J. A. Flores-Livas, *Nature (London)* **578**, 66 (2020).
- [7] J. A. Flores-Livas, L. Boeri, A. Sanna, G. Profeta, R. Arita, and M. Eremets, *Phys. Rep.* **856**, 1 (2020).
- [8] T. Bi, N. Zarifi, T. Terpstra, and E. Zurek, in *Reference Module in Chemistry, Molecular Sciences and Chemical Engineering* (Elsevier, Amsterdam, 2019).
- [9] C. J. Pickard, I. Errea, and M. I. Eremets, *Annu. Rev. Condens. Matter Phys.* **11**, 57 (2020).
- [10] L. Zhang, Y. Wang, J. Lv, and Y. Ma, *Nat. Rev. Mater.* **2**, 17005 (2017).
- [11] A. R. Oganov, C. J. Pickard, Q. Zhu, and R. J. Needs, *Nat. Rev. Mater.* **4**, 331 (2019).
- [12] E. Snider, N. Dasenbrock-Gammon, R. McBride, M. Debessai, H. Vindana, K. Vencatasamy, K. V. Lawler, A. Salamat, and R. P. Dias, *Nature (London)* **586**, 373 (2020).
- [13] J. E. Hirsch and F. Marsiglio, *arXiv:2010.10307*.
- [14] J. E. Hirsch and F. Marsiglio, *Phys. C: Supercond. Appl.* **584**, 1353866 (2021).
- [15] J. E. Hirsch and F. Marsiglio, *Phys. Rev. B* **103**, 134505 (2021).
- [16] E. F. Talantsev, *Supercond. Sci. Technol.* **34**, 034001 (2021).
- [17] M. Dogan and M. L. Cohen, *Phys. C: Supercond. Appl.* **583**, 1353851 (2021).
- [18] Y. Sun, Y. Tian, B. Jiang, X. Li, H. Li, T. Iitaka, X. Zhong, and Y. Xie, *Phys. Rev. B* **101**, 174102 (2020).
- [19] W. Cui, T. Bi, J. Shi, Y. Li, H. Liu, E. Zurek, and R. J. Hemley, *Phys. Rev. B* **101**, 134504 (2020).
- [20] Y. Ge, F. Zhang, R. P. Dias, R. J. Hemley, and Y. Yao, *Mater. Today Phys.* **15**, 100330 (2020).
- [21] S. X. Hu, R. Paul, V. V. Karasiev, and R. P. Dias, *arXiv:2012.10259*.
- [22] The compositional and configurational space of C-S-H was explored using the minima-hopping method [42–45]. The representative compositions of the ternary phase diagram were carried out with different formula units (containing up to 48 atoms) and carried out under pressure. Energy, atomic forces, and stresses were evaluated using the density-functional theory (further details are included in the Supplemental Material [24]).
- [23] https://github.com/TCWang-96/C-S-H_ternary_compounds.
- [24] See Supplemental Material at <http://link.aps.org/supplemental/10.1103/PhysRevB.104.064510> for chemical exploration and structure prediction in the C-S-H convex hull, electronic structure and phonons for the doped phases, and theoretical and computational details of the superconductivity calculation based on the Migdal-Eliashberg theory as well as the McMillan-Allen-Dynes formula.
- [25] We note that the contribution of ZPE is important in the first-principles studies of the stability of structures and the determination of the most stable structures for H_3S [39] and LaH_{10} [6] at high pressures. However, ZPE plays a minor role in the analysis of the thermodynamic convex hull [46]. Thus, we assume that its contribution will not affect the trends in the convex hull, and it is neglected in this study.
- [26] J. A. Flores-Livas, T. Wang, T. Nomoto, T. Koretsune, Y. Ma, R. Arita, and M. Eremets, *arXiv:2010.06446*.
- [27] R. Akashi, *Phys. Rev. B* **101**, 075126 (2020).
- [28] W. L. McMillan, *Phys. Rev.* **167**, 331 (1968).
- [29] P. B. Allen and R. C. Dynes, *Phys. Rev. B* **12**, 905 (1975).
- [30] P. B. Allen and B. Mitrović, *Theory of Superconducting T_c* , Solid State Physics Vol. 37 (Academic, Cambridge, MA, 1983), pp. 1–92.
- [31] P. E. Blöchl, O. Jepsen, and O. K. Andersen, *Phys. Rev. B* **49**, 16223 (1994).
- [32] T. Koretsune and R. Arita, *Comput. Phys. Commun.* **220**, 239 (2017).
- [33] T. Wang, T. Nomoto, Y. Nomura, H. Shinaoka, J. Otsuki, T. Koretsune, and R. Arita, *Phys. Rev. B* **102**, 134503 (2020).
- [34] W. Sano, T. Koretsune, T. Tadano, R. Akashi, and R. Arita, *Phys. Rev. B* **93**, 094525 (2016).
- [35] To study the doping effect of C atoms in $\text{C}_x\text{S}_{1-x}\text{H}_3$, we used (i) the virtual crystal approximation (VCA) [47,48] and performed a thorough examination of $\text{C}_x\text{S}_{1-x}\text{H}_3$ with x ranging from 1% to 8.3%, in which for the virtual atom we use the potential $V_{\text{VCA}} = xV_{\text{C}} + (1-x)V_{\text{S}}$; (ii) the actual supercell calculation for C atoms doping with an 8% ratio. We use QUANTUM ESPRESSO [49] for the density functional theory (DFT) and density functional perturbation theory (DFPT) calculations [50], with the exchange-correlation functional proposed by Perdew, Burke, and Ernzerhof [51]. For C and S atoms, the optimized norm-conserving Vanderbilt pseudopotential (ONCVSP) [52] was employed. For the H atom, we use the ultrasoft pseudopotentials [53] provided in PSLibrary [54]. To generate V_{VCA} , we use the tool VIRTUALV2.X implemented in QUANTUM ESPRESSO. For the DFT calculation, the cutoff energy of the plane waves for wave-function expansion is set to be 80 Ry, and the cutoff of the charge density is 320 Ry. For calculations using V_{VCA} , we use an $18 \times 18 \times 18k$ mesh and a $9 \times 9 \times 9q$ mesh for the DFPT calculation and a $36 \times 36 \times 36k$ mesh for the electron-phonon calculation. For the electron-phonon calculation and the Eliashberg calculation, the electronic eigenenergies and wave functions are calculated using a $36 \times 36 \times 36k$ mesh. We have also performed a supercell calculation for $\text{C}_x\text{S}_{1-x}\text{H}_3$ with $x = 0.083$, using a $3 \times 2 \times 2$ supercell containing 48 atoms. The supercell calculation is performed on a $6 \times 6 \times 6k$ mesh and a $3 \times 3 \times 3q$ mesh for the DFPT calculation, and a $12 \times 12 \times 12k$ mesh is employed for the electron-phonon interaction and Eliashberg calculation. In the Eliashberg calculation, we use a random phase approximation (RPA)-type static Coulomb kernel, with a $6 \times 6 \times 6k$ mesh and a $3 \times 3 \times 3q$ mesh for the Coulomb calculation. To accelerate the Migdal-Eliashberg calculation we use the IRBASIS library [55] to generate the intermediate representation (IR) basis functions for the Green's function as well as the sparse sampling method for the Matsubara frequencies. More theoretical and computational details of superconductivity calculation can be found in the Supplemental Material [24].
- [36] A. J. Flores-Livas, A. Sanna, and E. Gross, *Eur. Phys. J. B* **89**, 63 (2016).
- [37] R. Akashi, M. Kawamura, S. Tsuneyuki, Y. Nomura, and R. Arita, *Phys. Rev. B* **91**, 224513 (2015).
- [38] R. Akashi, W. Sano, R. Arita, and S. Tsuneyuki, *Phys. Rev. Lett.* **117**, 075503 (2016).
- [39] I. Errea, M. Calandra, C. J. Pickard, J. R. Nelson, R. J. Needs, Y. Li, H. Liu, Y. Zhang, Y. Ma, and F. Mauri, *Nature (London)* **532**, 81 (2016).
- [40] V. S. Minkov, V. B. Prakapenka, E. Greenberg, and M. I. Eremets, *Angew. Chem., Int. Ed.* **59**, 18970 (2020).

- [41] S. Mozaffari, D. Sun, V. S. Minkov, A. P. Drozdov, D. Knyazev, J. B. Betts, M. Einaga, K. Shimizu, M. I. Eremets, L. Balicas *et al.*, *Nat. Commun.* **10**, 2522 (2019).
- [42] S. Goedecker, *J. Chem. Phys.* **120**, 9911 (2004).
- [43] M. Amsler and S. Goedecker, *J. Chem. Phys.* **133**, 224104 (2010).
- [44] J. A. Flores-Livas, M. Amsler, C. Heil, A. Sanna, L. Boeri, G. Profeta, C. Wolverton, S. Goedecker, and E. K. U. Gross, *Phys. Rev. B* **93**, 020508(R) (2016).
- [45] J. A. Flores-Livas, *J. Phys.: Condens. Matter* **32**, 294002 (2020).
- [46] I. Errea, M. Calandra, C. J. Pickard, J. Nelson, R. J. Needs, Y. Li, H. Liu, Y. Zhang, Y. Ma, and F. Mauri, *Phys. Rev. Lett.* **114**, 157004 (2015).
- [47] L. Nordheim, *Ann. Phys.* **401**, 607 (1931).
- [48] L. Bellaiche and D. Vanderbilt, *Phys. Rev. B* **61**, 7877 (2000).
- [49] P. Giannozzi, O. Andreussi, T. Brumme, O. Bunau, M. B. Nardelli, M. Calandra, R. Car, C. Cavazzoni, D. Ceresoli, M. Cococcioni *et al.*, *J. Phys.: Condens. Matter* **29**, 465901 (2017).
- [50] S. Baroni, S. de Gironcoli, A. Dal Corso, and P. Giannozzi, *Rev. Mod. Phys.* **73**, 515 (2001).
- [51] J. P. Perdew, K. Burke, and M. Ernzerhof, *Phys. Rev. Lett.* **77**, 3865 (1996).
- [52] D. R. Hamann, *Phys. Rev. B* **88**, 085117 (2013).
- [53] D. Vanderbilt, *Phys. Rev. B* **41**, 7892 (1990).
- [54] A. Dal Corso, *Comput. Mater. Sci.* **95**, 337 (2014).
- [55] N. Chikano, K. Yoshimi, J. Otsuki, and H. Shinaoka, *Comput. Phys. Commun.* **240**, 181 (2019).